国立大学法人電気通信大学 / The University of Electro-Communications

Motion control of a snake robot moving between two non-parallel planes

著者（英）	Mizuki Nakajima, Motoyasu Tanaka, Kazuo Tanaka, Fumitoshi Matsuno
journal or publication title	Advanced Robotics
volume	32
number	10
page range	559-573
year	2018-04-08
URL	http://id.nii.ac.jp/1438/00009019/

doi: 10.1080/01691864.2018.1458653

To appear in *Advanced Robotics*
Vol. 00, No. 00, June 2017, 1–18

FULL PAPER

Motion control of a snake robot moving between two non-parallel planes

Mizuki Nakajima[a]*, Motoyasu Tanaka[a], Kazuo Tanaka[a], and Fumitoshi Matsuno[b]

[a] *The University of Electro-Communication, 1-5-1 Chofugaoka, Chofu, Tokyo, Japan*;
[b] *Kyoto University, Kyotodaigaku-Katsura, Sakyo-ku, Kyoto, Japan*;

(*v1.0 released June 2017*)

A control method that makes the head of a snake robot follow an arbitrary trajectory on two non-parallel planes, including coexisting sloped and flat planes, is presented. We clarify an appropriate condition of contact between the robot and planes and design a controller for the part of the robot connecting the two planes that satisfies the contact condition. Assuming that the contact condition is satisfied, we derive a simplified model of the robot and design a controller for trajectory tracking of the robot's head. The controller uses kinematic redundancy to avoid violating the limit of the joint angle and a collision between the robot and the edge of a plane. The effectiveness of the proposed method is demonstrated in experiments using an actual robot.

Keywords: Snake robot, Slope, Redundancy, Trajectory tracking

1. Introduction

Snake robots have an elongated body, such as that of a snake, and can travel over various terrain; e.g., snake robots can travel along narrow paths, over uneven terrain, under water, and along pipes. Snake robots are expected to be actively used in search and rescue operations at disaster sites where there is varying terrain. The body of a snake has an anisotropic friction condition under which the body is slippery in the propulsive direction and not slippery in the direction orthogonal to the trunk. Many robots having passive wheels that satisfy the anisotropic friction condition have been researched and developed [1–7]. Additionally, because it is difficult to control snake robots that have many joints, many works on motion and control, such as path following and trajectory tracking, have been performed. Most of the works assume that the terrain is a flat plane. In recent years, however, studies have been conducted for terrain that is curved or rough; e.g., a step [8–11], two parallel planes [12, 13], a smooth hill [14], and a cylinder [15–20]. Several of the works considered a step or stairs comprising many planes [8–10, 15]. Yamada succeeded in having a snake robot with powered wheels climb a step [8]. Lipkin succeeded in having a snake robot climb stairs, using a preplanned body curve that was heuristically designed [15]. However, the robot acts according to preplanned motion, and tracking to an arbitrary trajectory is not guaranteed.

A slender multi-connected robot, such as a snake robot, has sensors that measure the environment (e.g., a vision or lidar sensor mounted on the head) and plans its motion according to the measurements [21–25]. When the robot is remotely controlled, it is intuitive and easy for an operator to control the robot according to the head position and attitude because the sensors are usually attached to the head. Tracking control of the robot's head to an arbitrary trajectory is therefore effective from the viewpoint of remote control. We previously proposed a

*Corresponding author. Email: mizuki.nakajima@rc.mce.uec.ac.jp

controller by which the head of the robot follows an arbitrary trajectory across two ascending or two descending parallel planes [9, 10]. However, two planes are not always parallel for a step in real-world scenes. No research has proposed a control method that guarantees the convergence of controlled variables theoretically for such terrain. It is thus necessary to establish a control method for motion across two non-parallel planes.

Previous studies have considered a slope as the environment [26–28]. Optimal propulsive parameters for a slope have been calculated [26], motion on a slope has been accomplished by the online optimization of parameters of central pattern generators[27], and a stability index of sidewinding motion on a slope has been proposed [28]. The cited studies considered only one sloped plane and did not mention the transition from a horizontal plane to a sloped plane. In contrast, Gong realized travel across various sloped planes by selecting optimum propulsion parameters [29]. However, the position of the head or center of gravity of the robot could not be explicitly controlled because the motion was a sidewinding motion.

The biped robot [30] and the four wheel-legged robot [31] can move on two non-parallel planes. However, their control methods cannot be applied to the snake robot because the structures and propulsion principles of these robots are different from those of snake robots.

Against the background described above, we aim to realize the trajectory tracking control of a snake robot on two non-parallel planes. The contribution of the paper is to propose a control method that enables the snake robot to move between two non-parallel planes, in which the robot can not move by using the previous method in [9]. We first clarify the contact conditions that propel the robot across terrain, and propose a control method that satisfies the conditions. We then simplify the control model on the assumption that the above conditions are satisfied. We finally verify the effectiveness of the proposed method in experiments using an actual robot.

2. Problem formulation

2.1 *Snake robot and two non-parallel planes*

We use the snake robot shown in Figure 1. The snake robot consists of $2n$ links connected by $2n-1$ joints. The rotation axes of the adjacent joints are orthogonal. Let l_i be the length of the i-th link, ψ_i be the relative angle between the i-th link and $i+1$-th link, and ψ_i be controlled directly by the i-th joint. Joints $1, 3, \cdots, 2n-1$-th are the yaw rotational joints while joints $2, 4, \cdots, 2(n-1)$-th are the pitch rotational joints. We set $\boldsymbol{\psi} = \left[\psi_1, \psi_2, \cdots, \psi_{2n-1}\right]^{\mathrm{T}} \in \mathbb{R}^{2n-1,1}$. The snake robot has pairs of passive wheels, and a wheel axis is the same as the rotational axis of the pitch joint. We assume that each wheel does not skid. Note that the assumption is not satisfied in the case where the lateral force applied to the wheel is large, e.g., the acceleration of the motion is large and slope angle of planes is steep. If a wheel does not skid, its velocity is constrained such that the velocity in the direction of the wheel axis is zero. The snake robot propels itself by lateral undulation using the velocity constraint [5]. The mechanical structure of the robot is the same as that in previous research [6, 9], and the robot can climb steps and stairs as in [9] and has three-dimensional trajectory tracking of its head as in [6]. Figure 1(b) shows the model of the robot.

Figure 2 shows two non-parallel planes. We refer to the plane in the direction that the robot travels as the front plane, and the other plane as the rear plane. We denote by Σ_f the coordinate system at an arbitrary point on the front plane, and by Σ_r the coordinate system at an arbitrary point on the rear plane. The reference coordinate system Σ_o coincides with Σ_r. Let $\boldsymbol{p}_{\mathrm{front}} \in \mathbb{R}^{3,1}$ and $\boldsymbol{p}_{\mathrm{rear}} \in \mathbb{R}^{3,1}$ be the origins of these coordinate systems, respectively. As shown in Fig. 2, the z axis of a coordinate system coincides with the normal vector of each plane, the x axis is positive in the direction of travel of the robot. The orientation of Σ_f relative to Σ_r is represented as $\boldsymbol{\theta}_{\mathrm{front}} = \left[\theta_{\mathrm{roll}}, \theta_{\mathrm{pitch}}, \theta_{\mathrm{yaw}}\right]^{\mathrm{T}}$. Here, the rotation matrix representing Σ_f relative to Σ_r is expressed

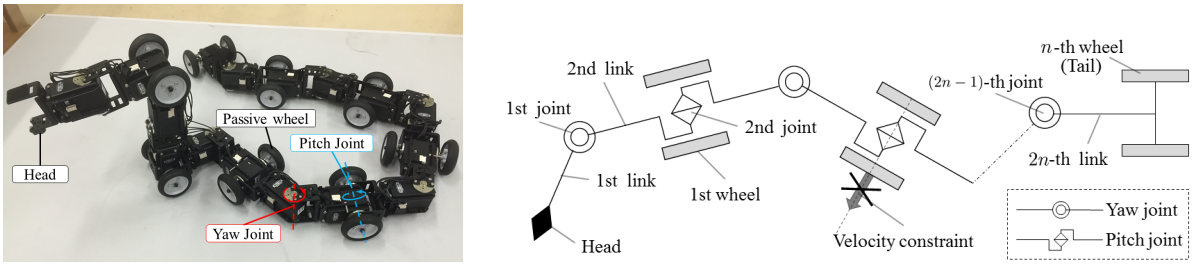

(a) Experimental robot

(b) Model

Figure 1. Snake robot

by

$$\boldsymbol{R}_f = \boldsymbol{R}_z(\theta_{\text{yaw}})\ \boldsymbol{R}_y(\theta_{\text{pitch}})\ \boldsymbol{R}_x(\theta_{\text{roll}})\ , \tag{1}$$

where $\boldsymbol{R}_i(\theta) \in \mathbb{R}^{3,3}$ is the matrix representing the rotation θ around the i axis of the reference coordinate system. We assume that these coordinate systems are fixed. In this paper, we assume that the parameter of environment and the position and attitude of the robot's head are given. This assumption can be satisfied by measuring or estimating these parameters by using sensors (e.g., motion capture system). In contrast, on the parallel planes in which the height and relative position between the robot and a step are unknown, we realized propulsion of the robot by installing LRF at the head as [10]. If the robot can measure or estimate the relative position and orientation to the non-parallel planes by using sensors(e.g., LRF), the robot can move between the unknown non-parallel planes.

In such environment, it is possible that the snake robot slides down a slope. The condition whether the robot slides down or not are represented by the relationship of forces between the robot and planes. It is possible that the normal force and frictional force of each wheel are calculated based on the dynamic model of the snake robot. However the dynamic model has not been derived because the control method in the paper is based on the kinematic model. The control method considering the avoidance of sliding down, e.g., using forces which are calculated by the dynamic model or directly measured by force sensors, is one of future works. In this paper, we derive a model and design a controller assuming that the slope angle is small and the wheel does not skid.

The purpose of the paper is to realize propulsion across two planes as shown in Fig. 2(c). We refer to the part of the whole robot in contact with the front plane as the front plane part, the part in contact with the rear plane as the rear plane part, the part from the rear end of the front plane part to the front end of the rear plane part as the connection part. The control objective is to make the head of the robot follow an arbitrary trajectory on the front plane. Both wheels of a pair of passive wheels need to be in proper contact with each plane for propulsion in the environment as shown in Fig. 2(c); this is ensured by the velocity constraint of the wheels. The robot propels itself by undulation of its whole self in addition to the above proper contact of the wheels. Therefore, in the case of propulsion on two non-parallel planes, it is necessary for the robot to maintain contact with the planes by adopting an appropriate posture, and to properly undulate using its whole body.

2.2 *Motion flow*

Figure 3 shows the flow of the motion in the assumed environment. We refer to the transition from motion on the rear plane to motion when straddling the two planes as *head adaptive motion*(A–B), and the motion when straddling the two planes by shifting the connection part

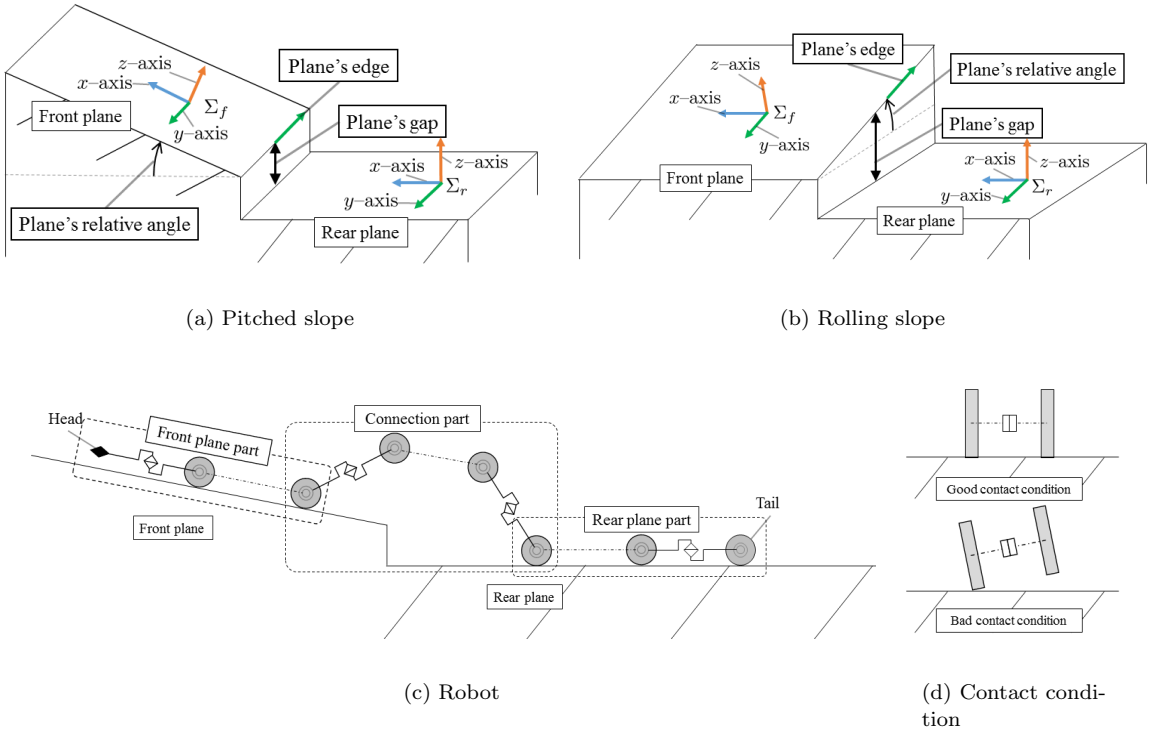

(a) Pitched slope

(b) Rolling slope

(c) Robot

(d) Contact condition

Figure 2. Two non-parallel planes and coordinate systems

as *motion for straddling two planes*(C–E). The state of the robot shifts from motion on the rear plane to motion for straddling two planes through head adaptive motion. In head adaptive motion, the head of the robot and the first pair of wheels are in proper contact with the front plane. Next, the robot propels itself by motion for straddling two planes. In the motion, the wheels come into proper contact with each plane through control of the connection part, and the position and attitude of the head track an arbitrary trajectory through control of the other (flat) part. Then, as the motion advances, the connection part sequentially propagates backward. We refer to the above propagation as *propagation of the connection part*. Propagation consists of two phases: 1) transition of the rear end of the connection part and 2) transition of the front end of the connection part. The robot repeats the propagation of the connection part and finally switches the controller to the method for motion on a flat plane. This paper deals with the head adaptive motion, the motion for straddling two planes, and the propagation of the connection part.

If we design the kinematic model of motion for straddling two planes using a three-dimensional model, the model will be complex because the nonholonomic constraint of the wheel should be represented as a three-dimensional constraint. We therefore simplify the control model using two models; one model is used to maintain contact with the two planes while the other is used to generate undulation of the whole robot. Sections 3 and 4 respectively derive the model for maintaining contact with the two planes and the model for generating undulation of the whole robot.

3. Model of the connection part

Figure 4 shows the model of the connection part. Let the i_{fe}-th wheel of all wheels of the robot be a front-end wheel of the connection part, the i_{re}-th wheel be a rear-end wheel of the connection part, and the i_{fe}-th wheel to the i_{re}-th wheel be the connection-part wheels (where the total

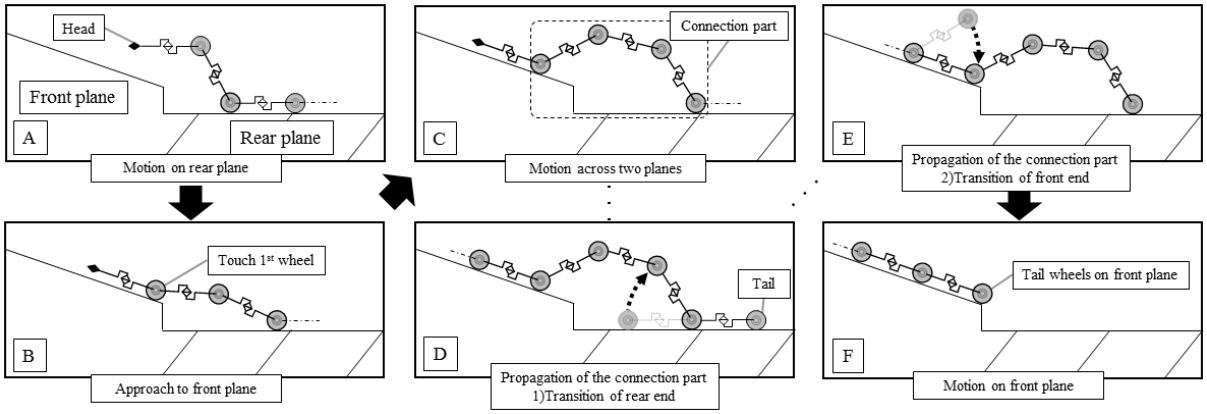

Figure 3. Motion flow

number of wheels is n_c). $(i_{\mathrm{fe}}+i-1)$-th wheel of the whole robot is described as the i-th wheel of the connection part. Let ${}^c\boldsymbol{p}_i \in \mathbb{R}^{3,1}$ be the three-dimensional position of the i-th wheel of the connection part relative to the reference coordinate system, and $\boldsymbol{w}_f = \left[x_f, y_f, \theta_f\right]^{\mathrm{T}}$ be the position and attitude of the front-end wheel of the connection part projected onto the $x-y$ plane of Σ_f, and $\boldsymbol{w}_r = \left[x_r, y_r, \theta_r\right]^{\mathrm{T}}$ be the position and attitude of the rear-end wheel of the connection part projected onto the $x-y$ plane of Σ_r. $\boldsymbol{w}_f$ is calculated from the position and attitude of the robot's head and the angles of the front-plane joints. $\boldsymbol{w}_r$ is calculated from $\boldsymbol{w}_f$ and the angles of the connection-part joints. Additionally, as shown in Fig. 4, let $\boldsymbol{a}_i \in \mathbb{R}^{3,1}$ be the unit vector directed from ${}^c\boldsymbol{p}_i$ toward the center of the left wheel, and $\boldsymbol{l}_i \in \mathbb{R}^{3,1}$ be the unit vector representing the orientation of the link behind the wheel. Let the $2i_{\mathrm{fe}}$-th joint to the $2i_{\mathrm{re}}$-th joint be the connection-part joints, and $\boldsymbol{\psi}_c = \left[\psi_{2i_{\mathrm{fe}}}, \cdots, \psi_{2i_{\mathrm{re}}}\right]^{\mathrm{T}} \in \mathbb{R}^{m_c,1}$ be the angles of the connection-part joints. The total number of the connection-part joints is described as $m_c = 2(i_{\mathrm{re}} - i_{\mathrm{fe}}) + 1$. The i-th element of $\boldsymbol{\psi}_c$ is denoted ${}^c\psi_i$. $(2i_{\mathrm{fe}+i-1})$-th joint of the whole robot is described as the i-th connection-part joint, and $\psi_{2i_{\mathrm{fe}}+i-1}$ is described as the ${}^c\psi_i$. Here, we assume that the front-end wheels of the connection part are properly in contact with the front plane. Thus, ${}^c\boldsymbol{p}_i$ is calculated from $\boldsymbol{w}_f$ and $\boldsymbol{\psi}_c$. Let d_i be the distance between ${}^c\boldsymbol{p}_i$ and the rear plane, ${}^a\phi_i$ be the relative angle between $\boldsymbol{a}_i$ and the rear plane, and ${}^l\phi_i$ be the relative angle between $\boldsymbol{l}_i$ and the rear plane as shown in Fig. 4. These are calculated as

$$d_i = \boldsymbol{n}_r^{\mathrm{T}}({}^c\boldsymbol{p}_i - \boldsymbol{p}_{\mathrm{rear}}) \ , \tag{2}$$

$${}^a\phi_i = \sin^{-1}(\boldsymbol{n}_r \cdot \boldsymbol{a}_i) \ , \tag{3}$$

$${}^l\phi_i = \sin^{-1}(\boldsymbol{n}_r \cdot \boldsymbol{l}_i) \ , \tag{4}$$

where $\boldsymbol{n}_r \in \mathbb{R}^{3,1}$ is the normal vector of the rear plane and the ranges of ${}^a\phi_i$ and ${}^l\phi_i$ are $[-\pi/2, \pi/2]$.

The objective in control of the connection part is for the wheels to be in proper contact with each plane. The robot controls the relative attitude between the front end and rear end of the connection part to achieve this objective. According to the above assumption, the front-end wheel of the connection part is properly in contact with the front plane. Thus, if the rear-end wheel of the connection part is properly in contact with the rear plane, all of the wheels are properly in contact with each plane. Here, the conditions that the rear-end wheel of the connection part is properly in contact with the rear plane are defined as

$$d_{n_c} = r_w \ , \tag{5}$$

$${}^a\phi_{n_c} = 0 \ . \tag{6}$$

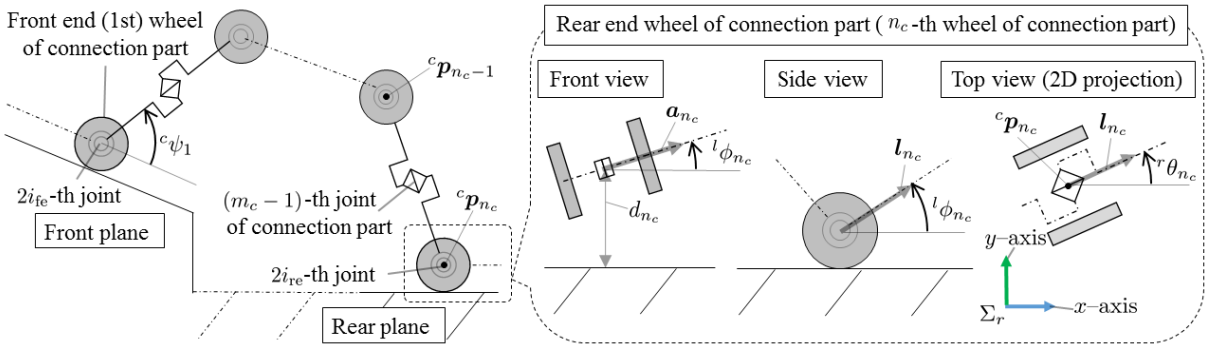

Figure 4. Model of the connection part

The additional condition that the rear-plane wheels are in contact with the rear plane is defined as

$$^l\phi_{n_c} = 0 \ . \tag{7}$$

Let $\boldsymbol{r} = \left[d_{n_c}, {}^a\phi_{n_c}, {}^l\phi_{n_c}\right]^{\mathrm{T}}$ be the controlled variable of the connection part, and $\boldsymbol{r}_d = \left[r_w, 0, 0\right]^{\mathrm{T}}$ be the target of $\boldsymbol{r}$. The rear-end wheel of the connection part has a velocity constraint in the axial direction of the wheel because it is in contact with the rear plane via an appropriate posture, and the velocity constraint is represented as

$$\dot{x}_r \sin\theta_r - \dot{y}_r \cos\theta_r = 0 \ . \tag{8}$$

Constraint (8) must be satisfied so that the wheel does not skid.

3.1 *Kinematic model of the connection part*

We define $\boldsymbol{q}_c = \left[\boldsymbol{w}_f^{\mathrm{T}}, \boldsymbol{\psi}_c^{\mathrm{T}}\right]^{\mathrm{T}} \in \mathbb{R}^{m_c+3,1}$. From (2)–(4), we can represent the kinematic relationship between $\boldsymbol{r}$ and $\boldsymbol{q}_c$ as

$$\dot{\boldsymbol{r}} = \boldsymbol{J}\dot{\boldsymbol{q}}_c \ , \tag{9}$$

where $\boldsymbol{J} = \partial\boldsymbol{r}/\partial\boldsymbol{q}_c \in \mathbb{R}^{3,m_c+3}$. By transforming (8), we obtain

$$\boldsymbol{D}\dot{\boldsymbol{q}}_c = 0 \ , \tag{10}$$

where $\boldsymbol{D} \in \mathbb{R}^{1,m_c+3}$. By rearranging (9)–(10), the kinematic model is obtained as

$$\begin{bmatrix}\dot{\boldsymbol{r}} \\ 0\end{bmatrix} = \boldsymbol{H}\dot{\boldsymbol{q}}_c \ , \tag{11}$$

where $\boldsymbol{H} = \left[\boldsymbol{J}^{\mathrm{T}}, \boldsymbol{D}^{\mathrm{T}}\right]^{\mathrm{T}} \in \mathbb{R}^{4,m_c+3}$.

3.2 *Head adaptive motion for the front plane*

In the case of head adaptive motion, we modify the kinematic model (11) partially, and use it for control of the robot. In the case of head adaptive motion, we refer to the part from the head of the robot to front end of the rear plane part as connection part. The robot consists of the connection part and the rear-plane part. Let n_h be the number of connection-part wheels used

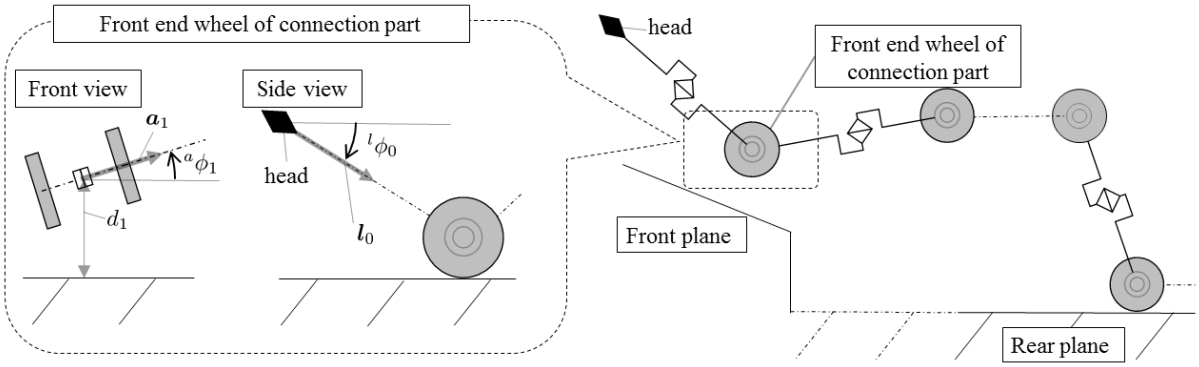

Figure 5. Model of head adaptive motion

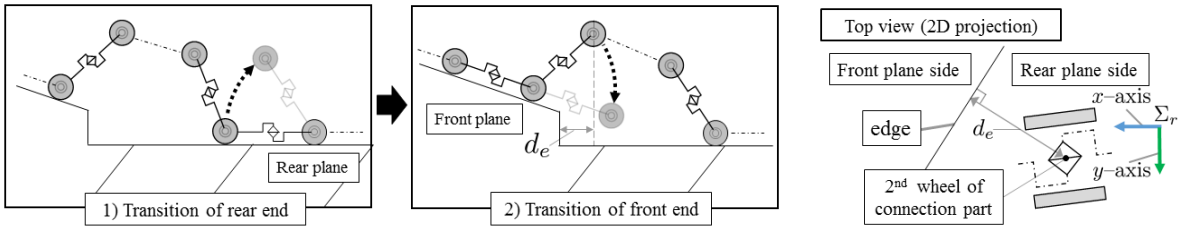

(a) Motion flow (b) Definition of d_e

Figure 6. Propagation of the connection part

in the head adaptive motion. The notations of ${}^c\boldsymbol{p}_i$ and $\boldsymbol{w}_r$ are the same as for the model of the connection part. We assume that the rear-end wheels of the connection part are in proper contact with the rear plane and $\boldsymbol{w}_r$ is constant. Let $\boldsymbol{l}_0$ be the unit vector representing the orientation of the first link behind as shown in Figure 5.

The control objective in head adaptive motion is for the head of the robot to be in proper contact with the front plane by controlling the relative attitude between the head and rear end of the connection part. According to the above assumption, the rear-end wheel of the connection part is in proper contact with the rear plane. The control objective is thus achieved by ensuring the head of the robot is in proper contact with the front plane. We define $\boldsymbol{r}_h = \left[d_1, {}^a\phi_1, {}^l\phi_0\right]^{\mathrm{T}}$ as the controlled variable for head adaptive motion, and $\boldsymbol{r}_{hd} = \left[r_w, 0, 0\right]^{\mathrm{T}}$ as the target value. If there is a large difference between the controlled variable and the target at the start of control, the control input becomes too large. We use a linearly interpolated value between the controlled variable at the start of control and the final target value as the target value at each time to reduce the magnitude of the control input. Derivation of the kinematic model and the input calculation are omitted because they are not greatly different from those in the case of the connection part.

3.3 *Propagation of the connection part*

Figure 3 C–E shows the robot transits to the front plane by propagating its connection part backward. The propagation of the connection part is achieved by the transition of the front end and rear end of the connection part backward. As shown in Figure 6(a), propagation of the connection part comprises two steps: 1) transition of the rear end of the connection part and 2) transition of the front end of the connection part. Each step starts and terminates by satisfying the start condition and end condition, respectively.

Transition of the rear end of the connection part is carried out by lifting the rear-end wheel

of the connection part. The start conditions of the transition are designed as

$$n_c < n_{c_{\max}} \ , \tag{12}$$

$$i_{\mathrm{re}} \leq n \ , \tag{13}$$

where $n_{c_{\max}}$ is the maximum number of connection-part wheels and is set in advance. When $n_{c_{\max}}$ increases, the redundancy of motion becomes high. In contrast, when the $n_{c_{\max}}$ increases, the number of wheels which are lifted increases. If the number of wheels which are lifted is large, the risk of falls and sliding increases. Condition (12) prevents the robot from falling by increasing the number of connection-part wheels. Condition (13) means that all rear-plane wheels are lifted. If the start conditions (12) and (13) are satisfied, we set $i_{\mathrm{re}} = i_{\mathrm{re}} + 1$ for transition of the rear end of the connection part backward. In conjunction with the transition, the elements of $\boldsymbol{r}$ replace the components of the next wheel. For example, in the transition from $i_{\mathrm{re}} = j$ to $i_{\mathrm{re}} = j + 1$, the elements of $\boldsymbol{r}$ before transition consist of the distance and relative angle between the j-th wheel and rear plane, and elements of $\boldsymbol{r}$ after transition consist of the distance and relative angle between the $j + 1$-th wheel and rear plane. The elements of model (11) are also replaced.

In the case of $i_{\mathrm{re}} = n$, the rear-plane wheels are only the rear-end wheels of the connection part. Then, ${}^{l}\phi_{n_c}$ is removed from the set of controlled variables for the connection part because it is only related to the condition that the rear-plane wheels except for the connection-part wheels are in proper contact with the rear plane. Additionally, in the case of $i_{\mathrm{re}} > n$, there are no rear-plane wheels. Thus, the relative attitude of the connection part is not controlled. The calculation of the actual control input at this time will be described later.

As shown in Fig. 6(a)–2), transition of the front end of the connection part is carried out by making the second wheel of the connection part come into contact with the front plane. The start conditions of the transition are designed as

$$d_e < \varepsilon_d \ , \tag{14}$$

$$n_c > n_{c_{\min}} \ , \tag{15}$$

where d_e is the signed distance between the edge of the front plane and the position of the second wheel of the connection part projected onto the $x-y$ plane of the Σ_r coordinate system as shown in Fig. 6(b), ε_d is a small arbitrary constant representing the distance at which the transition starts, and $n_{c_{\min}}$ is the minimum number of connection-part wheels. The $n_{c_{\min}}$ is determined from the degree of freedom required for propulsion and propagation of connection part. Note that condition (15) is not considered in the case that $i_{\mathrm{re}} > n$. Incidentally, d_{e} is positive when the position of the second wheel of the connection part projected onto the $x-y$ plane of the reference coordinate system is on the rear-plane side. When start conditions (14) (15) are satisfied, we add ${}^{c}\psi_1$ to the set of controlled variables and use $\hat{\boldsymbol{r}} = \left[\boldsymbol{r}^{\mathrm{T}}, {}^{c}\psi_1\right]^{\mathrm{T}}$ and $\hat{\boldsymbol{r}}_d = \left[\boldsymbol{r}_d^{\mathrm{T}}, 0\right]^{\mathrm{T}}$ as the controlled variable and its target value, respectively. The modified model is presented as

$$\begin{bmatrix} \dot{\hat{\boldsymbol{r}}} \\ 0 \end{bmatrix} = \hat{\boldsymbol{H}} \dot{\boldsymbol{q}}_c \ , \tag{16}$$

$$\hat{\boldsymbol{H}} = \begin{bmatrix} \boldsymbol{J} \\ 0\,0\,0\,1\,0 \cdots 0 \\ \boldsymbol{D} \end{bmatrix} \ , \tag{17}$$

where $\hat{\boldsymbol{H}} \in \mathbb{R}^{5, m_c+3}$. The end condition is then designed as

$${}^{c}\psi_1 < \varepsilon_\psi \ . \tag{18}$$

When condition (18) is satisfied, we set $i_{\mathrm{fe}} = i_{\mathrm{fe}} + 1$ for transition of the front end of the

connection part backward, and we use model (11) after the transition. By repeating the above operation until the front-end wheel of the connection part coincides with the tail of the robot, the whole robot transits to the front plane.

Elements included in the controlled variable discretely are switched by the transition of the wheel. There is then a risk that the controller generates too large an input in the case that there is a large difference between the controlled variable and the target value just after the switch of the controlled variable. We thus use the linearly interpolated value between the controlled variable just after the switch and the final target value as the target value at each time to reduce the magnitude of the control input.

4. Model of the flat part for trajectory tracking

In the initial state of the motion for straddling two planes, the head and first wheel of the robot properly touch the front plane as in Fig. 3–B. The snake robot propels itself with lateral undulation under velocity constraints due to the passive wheels. The control objective in the motion for straddling two planes is to make the head of the snake robot track the desired trajectory on the front plane. We assume that wheels are in proper contact with each plane owing to the control of the connection part. Here, the position and attitude of the front-plane part and rear-plane part are expressed as the two-dimensional position and attitude projected on each plane. Figure 7 shows the model of each plane part projected on each plane. Let the first wheel to the i_{fe}-th wheel (a total of n_f wheels) be the front plane wheels, and the $(i_{\mathrm{re}}+1)$-th wheel to the n-th wheel (a total of n_r wheels) be the rear plane wheels. $(i_{\mathrm{re}}+i)$-th wheel of the whole robot is described as the i-th rear-plane wheel. Additionally, let the first joint to the $(2i_{\mathrm{fe}}-1)$-th joint be the front-plane joints, and the $(2i_{\mathrm{re}}+1)$-th joint to the $(2n-1)$-th joint be the rear-plane joints. We assume that the pitch joints included in the front-plane joints and rear-plane joints are controlled to have zero joint angle and therefore do not operate. This assumption is needed as each plane part is in proper contact with each plane. Let the yaw joints angle included in the front-plane part be $\boldsymbol{\psi}_f = \left[\psi_1, \psi_3, \cdots, \psi_{2i_{\mathrm{fe}}-1}\right]^{\mathrm{T}} \in \mathbb{R}^{n_f,1}$, and the yaw joints angle included in the rear plane part be $\boldsymbol{\psi}_r = \left[\psi_{2i_{\mathrm{re}}+1}, \psi_{2i_{\mathrm{re}}+3}, \cdots, \psi_{2n-1}\right]^{\mathrm{T}} \in \mathbb{R}^{n_r,1}$. The i-th yaw joint angles of each plane part are described as the i-th elements of $\boldsymbol{\psi}_f$ and $\boldsymbol{\psi}_r$, and are denoted ${}^f\psi_i$ and ${}^r\psi_i$, respectively. The position and attitude of the i-th wheel $(i = 1, \cdots, n_f)$ of the front-plane part as seen in coordinate system Σ_f are denoted ${}^f\boldsymbol{p}_i = \left[{}^fx_i, {}^fy_i\right]^{\mathrm{T}}$ and ${}^f\theta_i$, respectively. ${}^f\boldsymbol{p}_i$ and ${}^f\theta_i$ are calculated from $\boldsymbol{w}_h = \left[x_h, y_h, \theta_h\right]^{\mathrm{T}}$, the position and attitude of the robot's head projected onto the $x-y$ plane of the Σ_f coordinate system, and the joint angle of the front-plane part $\boldsymbol{\psi}_f$. Furthermore, the position and attitude of the i-th wheel $(i = 1, \cdots, n_r)$ of the rear-plane part as seen in coordinate system Σ_r are denoted ${}^r\boldsymbol{p}_i = \left[{}^rx_i, {}^ry_i\right]^{\mathrm{T}}$ and ${}^r\theta_i$, respectively. ${}^r\boldsymbol{p}_i$ and ${}^r\theta_i$ are calculated from $\boldsymbol{w}_r = \left[x_r, y_r, \theta_r\right]^{\mathrm{T}}$, the position and attitude of the rear-end wheel of the connection part projected onto the $x-y$ plane of coordinate system Σ_r, and the joint angle of the rear-plane part $\boldsymbol{\psi}_r$. Accordingly, ${}^r\boldsymbol{p}_i$ and ${}^r\theta_i$ are calculated from $\boldsymbol{w}_h$, $\boldsymbol{\psi}_f$, $\boldsymbol{\psi}_c$, and $\boldsymbol{\psi}_r$. The velocity constraints due to the wheels of each plane part are presented as

$$\begin{cases} {}^f\dot{x}_i \sin {}^f\theta_i - {}^f\dot{y}_i \cos {}^f\theta_i = 0 & (i = 1, \cdots, n_f) \\ {}^r\dot{x}_i \sin {}^r\theta_i - {}^r\dot{y}_i \cos {}^r\theta_i = 0 & (i = 1, \cdots, n_r) \end{cases}. \tag{19}$$

Note that model (19) does not include the constraint of the rear-end wheel of the connection part because it is considered in the relative attitude control of the connection part as (8).

Let $\boldsymbol{w}_h$ be the vector of the controlled variables for trajectory tracking. By rearranging (19),

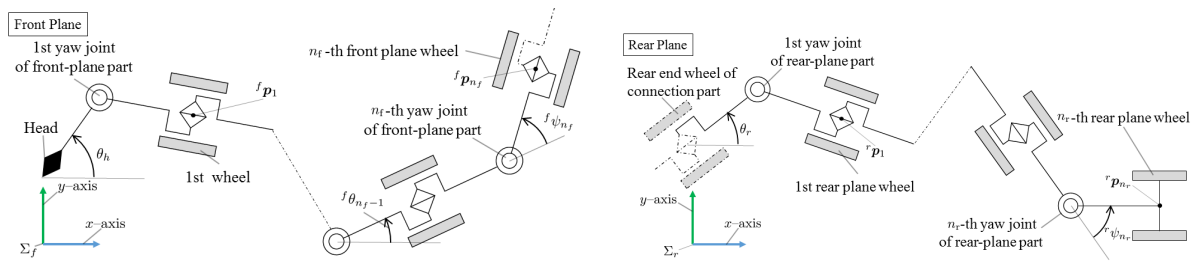

(a) Front-plane part (b) Rear-plane part

Figure 7. Model of each plane part

we obtain

$$\boldsymbol{A}_1\dot{\boldsymbol{w}}_h = \boldsymbol{B}_1\dot{\boldsymbol{\psi}}_f \ , \tag{20}$$

$$\boldsymbol{A}_2\dot{\boldsymbol{w}}_r = \boldsymbol{B}_2\dot{\boldsymbol{\psi}}_r \ , \tag{21}$$

where $\boldsymbol{A}_1 \in \mathbb{R}^{n_f,3}$, $\boldsymbol{B}_1 \in \mathbb{R}^{n_f,n_f}$, $\boldsymbol{A}_2 \in \mathbb{R}^{n_r,3}$, and $\boldsymbol{B}_2 \in \mathbb{R}^{n_r,n_r}$. Diagonal elements of $\boldsymbol{B}_1$ and $\boldsymbol{B}_2$ are constants determined by the structure of the robot, and they have an inverse matrix. Here, $\boldsymbol{w}_r$ is the position and attitude of the projection of ${}^c\boldsymbol{p}_{n_c}$ onto the $x-y$ plane of Σ_r, and ${}^c\boldsymbol{p}_{n_c}$ is calculated from $\boldsymbol{w}_h$, $\boldsymbol{\psi}_f$, and $\boldsymbol{\psi}_c$. Thus, $\boldsymbol{w}_r$ is obtained as

$$\dot{\boldsymbol{w}}_r = \boldsymbol{J}_{e_1}\dot{\boldsymbol{w}}_h + \boldsymbol{J}_{e_2}\dot{\boldsymbol{\psi}}_f + \boldsymbol{J}_{e_3}\dot{\boldsymbol{\psi}}_c \ , \tag{22}$$

where $\boldsymbol{J}_{e_1} \in \mathbb{R}^{3,3}$, $\boldsymbol{J}_{e_2} \in \mathbb{R}^{3,n_f}$, and $\boldsymbol{J}_{e_3} \in \mathbb{R}^{3,m_c}$. By substituting this equation into (21), we obtain

$$\boldsymbol{A}_2\boldsymbol{J}_{e_1}\dot{\boldsymbol{w}}_h = \begin{bmatrix} -\boldsymbol{A}_2\boldsymbol{J}_{e_2} & -\boldsymbol{A}_2\boldsymbol{J}_{e_3} & \boldsymbol{B}_2 \end{bmatrix} \begin{bmatrix} \dot{\boldsymbol{\psi}}_f \\ \dot{\boldsymbol{\psi}}_c \\ \dot{\boldsymbol{\psi}}_r \end{bmatrix} \ . \tag{23}$$

We set $\tilde{\boldsymbol{\psi}} = \left[\boldsymbol{\psi}_f^{\mathrm{T}}, \boldsymbol{\psi}_c^{\mathrm{T}}, \boldsymbol{\psi}_r^{\mathrm{T}}\right]^{\mathrm{T}}$. By rearranging (20–23), we obtain the kinematic model of the flat part as

$$\tilde{\boldsymbol{A}}\dot{\boldsymbol{w}}_h = \tilde{\boldsymbol{B}}\dot{\tilde{\boldsymbol{\psi}}} \ , \tag{24}$$

$$\tilde{\boldsymbol{A}} = \begin{bmatrix} \boldsymbol{A}_1 \\ \boldsymbol{A}_2\boldsymbol{J}_{e_1} \end{bmatrix} \ , \ \tilde{\boldsymbol{B}} = \begin{bmatrix} \boldsymbol{B}_1 & \boldsymbol{O} \\ -\boldsymbol{A}_2\boldsymbol{J}_{e_2} & -\boldsymbol{A}_2\boldsymbol{J}_{e_3} \ \boldsymbol{B}_2 \end{bmatrix} \ , \tag{25}$$

where $\tilde{\boldsymbol{A}} \in \mathbb{R}^{n_f+n_r,3}$ and $\tilde{\boldsymbol{B}} \in \mathbb{R}^{n_f+n_r,n_f+m_c+n_r}$.

5. Controller

Figure 8 is a schematic diagram of the proposed controller. We set $\boldsymbol{u} = \left[\boldsymbol{u}_f^{\mathrm{T}}, \boldsymbol{u}_c^{\mathrm{T}}, \boldsymbol{u}_r^{\mathrm{T}}\right]^{\mathrm{T}} = \left[\dot{\boldsymbol{\psi}}_f^{\mathrm{T}}, \dot{\boldsymbol{\psi}}_c^{\mathrm{T}}, \dot{\boldsymbol{\psi}}_r^{\mathrm{T}}\right]$. The control input $\boldsymbol{u}$ is designed from (11), (20), and (23).

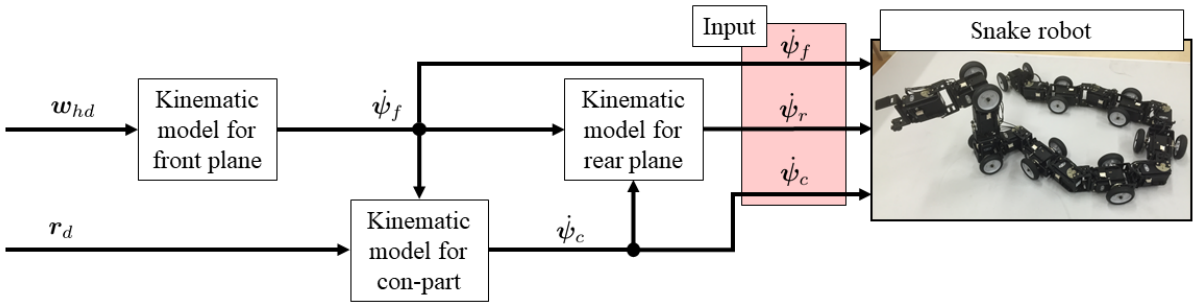

Figure 8. Control input

5.1 *Tracking controller*

Let $\boldsymbol{w}_{h_d}$ be the target position and attitude of the robot's head, and $\boldsymbol{K}_p = diag(\boldsymbol{k}_p) \in \mathbb{R}^{3,3}$ be a matrix that has positive gain for control of the flat part on diagonal elements. Firstly, $\dot{\boldsymbol{\psi}}_f$ is calculated from $\boldsymbol{w}_{h_d}$ and (20) as

$$\dot{\boldsymbol{\psi}}_f = \boldsymbol{B}_1^{-1}\boldsymbol{A}_1 \left\{ \dot{\boldsymbol{w}}_{h_d} + \boldsymbol{K}_p \left(\boldsymbol{w}_{h_d} - \boldsymbol{w}_h \right) \right\} \ . \tag{26}$$

Considering elements of $\boldsymbol{q}_c$, (11) is represented as

$$\begin{bmatrix} \dot{\boldsymbol{r}} \\ 0 \end{bmatrix} = \boldsymbol{H}_1 \dot{\boldsymbol{w}}_f + \boldsymbol{H}_2 \dot{\boldsymbol{\psi}}_c \ , \tag{27}$$

where $\boldsymbol{H}_1 \in \mathbb{R}^{4,3}$ and $\boldsymbol{H}_2 \in \mathbb{R}^{4,m_c}$. Additionally, the position and attitude of the front end of the connection part $\boldsymbol{w}_f$ are calculated from $\boldsymbol{w}_h$ and $\boldsymbol{\psi}_f$. The kinematic relationship among $\boldsymbol{w}_f$, $\boldsymbol{w}_h$, and $\boldsymbol{\psi}_f$ is expressed as

$$\dot{\boldsymbol{w}}_f = \boldsymbol{G}_1 \dot{\boldsymbol{w}}_h + \boldsymbol{G}_2 \dot{\boldsymbol{\psi}}_f \ , \tag{28}$$

where $\boldsymbol{G}_1 \in \mathbb{R}^{3,3}$, $\boldsymbol{G}_2 \in \mathbb{R}^{3,n_f}$. (11) is modified from (27) and (28) as

$$\begin{bmatrix} \dot{\boldsymbol{r}} \\ 0 \end{bmatrix} = \tilde{\boldsymbol{H}}_1 \dot{\boldsymbol{w}}_h + \tilde{\boldsymbol{H}}_2 \dot{\boldsymbol{\psi}}_f + \tilde{\boldsymbol{H}}_3 \dot{\boldsymbol{\psi}}_c \ , \tag{29}$$

$$\tilde{\boldsymbol{H}}_1 = \boldsymbol{H}_1 \boldsymbol{G}_1 \ , \ \tilde{\boldsymbol{H}}_2 = \boldsymbol{H}_1 \boldsymbol{G}_2 \ , \ \tilde{\boldsymbol{H}}_3 = \boldsymbol{H}_2 \ . \tag{30}$$

Here, $\tilde{\boldsymbol{H}}_1 \in \mathbb{R}^{4,3}$, $\tilde{\boldsymbol{H}}_2 \in \mathbb{R}^{4,n_f}$, $\tilde{\boldsymbol{H}}_3 \in \mathbb{R}^{4,m_c}$. Let $\boldsymbol{K}_c = diag(\boldsymbol{k}_c) \in \mathbb{R}^{3,3}$ be a matrix that has positive gain for control of the connection part on diagonal elements.

Secondly, $\dot{\boldsymbol{\psi}}_c$ is designed from (29) as

$$\dot{\boldsymbol{\psi}}_c = \tilde{\boldsymbol{H}}_3^{\dagger} \left\{ \begin{bmatrix} \dot{\boldsymbol{r}}_d + \boldsymbol{K}_c \left(\boldsymbol{r}_d - \boldsymbol{r} \right) \\ 0 \end{bmatrix} - \tilde{\boldsymbol{H}}_1 \left\{ \dot{\boldsymbol{w}}_{h_d} + \boldsymbol{K}_p \left(\boldsymbol{w}_{h_d} - \boldsymbol{w}_h \right) \right\} - \tilde{\boldsymbol{H}}_2 \dot{\boldsymbol{\psi}}_f \right\} + \left(\boldsymbol{I} - \tilde{\boldsymbol{H}}_3^{\dagger} \tilde{\boldsymbol{H}}_3 \right) \boldsymbol{l} \ , \tag{31}$$

where $\tilde{\boldsymbol{H}}_3^{\dagger}$ is the pseudo-inverse matrix of $\tilde{\boldsymbol{H}}_3$ and $\boldsymbol{l} \in \mathbb{R}^{m_c,1}$ is an arbitrary vector. The second term on the right-hand side of (31) is related to kinematic redundancy.

Finally, $\dot{\boldsymbol{\psi}}_r$ is designed from (23) as

$$\dot{\boldsymbol{\psi}}_r = \boldsymbol{B}_2^{-1}\boldsymbol{A}_2 \boldsymbol{J}_{e_1} \left\{ \dot{\boldsymbol{w}}_{h_d} + \boldsymbol{K}_p \left(\boldsymbol{w}_{h_d} - \boldsymbol{w}_h \right) \right\} + \boldsymbol{B}_2^{-1}\boldsymbol{A}_2 \left[\boldsymbol{J}_{e_2} \ \boldsymbol{J}_{e_3} \right] \begin{bmatrix} \dot{\boldsymbol{\psi}}_f \\ \dot{\boldsymbol{\psi}}_c \end{bmatrix} \ . \tag{32}$$

Substituting (26) and (32) into (24), the closed-loop system of the flat part is expressed as

$$\tilde{\boldsymbol{A}}\left\{\dot{\boldsymbol{w}}_{h_d} - \dot{\boldsymbol{w}}_h + \boldsymbol{K}_p\left(\boldsymbol{w}_{h_d} - \boldsymbol{w}_h\right)\right\} = \boldsymbol{0} \ . \tag{33}$$

If $\tilde{\boldsymbol{A}}$ is of full column rank, $\boldsymbol{w}_h = \boldsymbol{w}_{h_d}$ is concluded at $t \to \infty$. $\tilde{\boldsymbol{A}}$ is complicated because it is related to both the flat part and connection part. Thus, analysis of the rank of $\tilde{\boldsymbol{A}}$ is left as future work. Moreover, by substituting (31) into (11), the closed-loop system of the connection part is expressed as

$$\begin{bmatrix}\dot{\boldsymbol{r}}_d - \dot{\boldsymbol{r}} + \boldsymbol{K}_c\left(\boldsymbol{r}_d - \boldsymbol{r}\right) \\ 0\end{bmatrix} - \tilde{\boldsymbol{H}}_2\left\{\dot{\boldsymbol{w}}_{h_d} - \dot{\boldsymbol{w}}_h + \boldsymbol{K}_p\left(\boldsymbol{w}_{h_d} - \boldsymbol{w}_h\right)\right\} = \boldsymbol{0} \ , \tag{34}$$

where the second term on the left-hand side of (34) is zero according to (33). Thus, (34) is represented as

$$\dot{\boldsymbol{r}}_d - \dot{\boldsymbol{r}} + \boldsymbol{K}_c\left(\boldsymbol{r}_d - \boldsymbol{r}\right) = \boldsymbol{0} \ , \tag{35}$$

and $\boldsymbol{r} = \boldsymbol{r}_d$ is concluded at $t \to \infty$.

If $i_{\mathrm{re}} > n$, we design $\dot{\boldsymbol{\psi}}_f$ from (26) considering the velocity constraint of only the front-plane part. In this case, all connection-part joints are redundant components. The input of the connection part can thus be given arbitrarily as

$$\dot{\boldsymbol{\psi}}_c = \boldsymbol{l} \ . \tag{36}$$

5.2 *Kinematic redundancy*

Kinematic redundancy in (31) is used to avoid the angle limit violation of the connection-part joints and to avoid collision between the connection part and the environment. Let ψ_{lim} be the joint angle limit, and V_1 be the evaluation function related to joint limit avoidance of the connection part. V_1 is designed as

$$V_1 = \frac{1}{m_c}\sum_{i=1}^{m_c}\frac{\psi_{\mathrm{lim}}^2 - {}^c\psi_i^2}{\psi_{\mathrm{lim}}^2} \ . \tag{37}$$

Additionally, let V_2 be the evaluation function related to avoidance of collision between the connection part and environment. V_2 is designed as

$$V_2 = \frac{1}{n_c - 2}\sum_{i=2}^{n_c-1}\frac{d_r^2 - \left(d_i - d_d\right)^2}{d_r^2} \ , \tag{38}$$

where d_d and d_r are arbitrary constant values. d_d is the height which maximizes V_2. When d_d is set large value, the wheels are lifted high. d_r is a variable that determines the height which makes V_2 to zero. When d_i satisfies $d_i = d_d \pm d_r$, V_2 becomes zero. The weighted sum of V_1 and V_2 is designed as

$$V = \frac{g_1 V_1 + g_2 V_2}{g_1 + g_2} \ , \tag{39}$$

where g_1 and g_2 are positive constants. V is calculated from $\boldsymbol{w}_h$, $\boldsymbol{\psi}_f$, and $\boldsymbol{\psi}_c$. The time derivative of V is thus expressed as

$$\dot{V} = \frac{\partial V}{\partial \boldsymbol{w}_h}\dot{\boldsymbol{w}}_h + \frac{\partial V}{\partial \boldsymbol{\psi}_f}\dot{\boldsymbol{\psi}}_f + \frac{\partial V}{\partial \boldsymbol{\psi}_c}\dot{\boldsymbol{\psi}}_c \ . \tag{40}$$

Let $\boldsymbol{\eta} \in \mathbb{R}^{1,m_c}$ be $\partial V/\partial \boldsymbol{\psi}_c$, k_v be the positive gain for the evaluation function, and $\boldsymbol{l}$, the second term on the right-hand side of (31), be $k_v\boldsymbol{\eta}^{\mathrm{T}}$. k_v determines the magnitude of the input of the connection-part caused by redundancy. Substituting (26) and (31) into (40), $\dot{V}$ is obtained as

$$\dot{V} = \boldsymbol{E}_1\dot{\boldsymbol{w}}_h + \boldsymbol{E}_2\begin{bmatrix}\dot{\boldsymbol{r}}\\ 0\end{bmatrix} + k_v\boldsymbol{\eta}\left(\boldsymbol{I} - \tilde{\boldsymbol{H}}_3^{\dagger}\tilde{\boldsymbol{H}}_3\right)\boldsymbol{\eta}^{\mathrm{T}} \ , \tag{41}$$

$$\boldsymbol{E}_1 = \partial V/\partial \boldsymbol{w}_h + \left(\partial V/\partial \boldsymbol{\psi}_f - \boldsymbol{\eta}\tilde{\boldsymbol{H}}_3^{\dagger}\tilde{\boldsymbol{H}}_2\right)\boldsymbol{B}_1^{-1}\boldsymbol{A}_1 + \boldsymbol{\eta}\tilde{\boldsymbol{H}}_3^{\dagger}\tilde{\boldsymbol{H}}_1 \ , \tag{42}$$

$$\boldsymbol{E}_2 = \boldsymbol{\eta}\tilde{\boldsymbol{H}}_3^{\dagger} \ , \tag{43}$$

where $\boldsymbol{E}_1 \in \mathbb{R}^{1,3}$ and $\boldsymbol{E}_2 \in \mathbb{R}^{1,4}$. The first term on the right-hand side of (41) depends on controlled variables of the flat part, the second term depends on the controlled variable of the connection part, and the third term is related to kinematic redundancy. The third term is a nonnegative integer because $(\boldsymbol{I} - \tilde{\boldsymbol{H}}_3^{\dagger}\tilde{\boldsymbol{H}}_3) \geq \boldsymbol{0}$ [32]. The third term thus contributes to increasing V.

6. Experiment

We verified the effectiveness of the proposed control method by experiment using the snake robot shown in Fig .1(a). Figure 9 shows the experimental system. Parameters of the snake robot were $n = 9$, $l_i = 0.0905$ m ($i = 1, 2, \cdots, 2n$), $r_w = 0.029$ m, and $\psi_{\mathrm{lim}} = \pi/2$ radian. We set the control cycle as 0.2 s. Markers were attached to the head of the snake robot and the front plane, and the positions and attitudes of the markers were measured using a motion capture system. The normal vector of the front plane $\boldsymbol{n}_f$ was calculated from measured $\boldsymbol{p}_{\mathrm{front}}$ and $\boldsymbol{\theta}_{\mathrm{front}}$. Initial angles of the joint $\boldsymbol{\psi}_0$ were not given explicitly. We set values at the start of the experiment as $\boldsymbol{\psi}_0$. We defined $\boldsymbol{w}_{h_d}(t) = \left[x_{h_d}(t),\, y_{h_d}(t),\, \theta_{h_d}(t)\right]^{\mathrm{T}}$ as the target of the controlled variable at time t, denoted the time at the end of the head adaptive motion as t_0, and defined $\boldsymbol{w}_h$ at the end of the head adaptive motion as $\boldsymbol{w}_{h_0} = \left[x_{h_0},\, y_{h_0},\, \theta_{h_0}\right]^{\mathrm{T}}$. We designed $\boldsymbol{w}_{h_d}(t)$ as

$$x_{h_d}(t) = x_{h_0} + v_p(t - t_0) \ , \tag{44}$$

$$y_{h_d}(t) = y_{h_0} + A\sin\left(\frac{2\pi t}{T}\right) \ , \tag{45}$$

$$\theta_{h_d}(t) = \pi \ , \tag{46}$$

where $v_p > 0$ and A and T were arbitrary constants related to the target trajectory. We set $n_h = 3$, $n_{c_{\mathrm{min}}} = 3$, $n_{c_{\mathrm{max}}} = 4$, $\varepsilon_d = 0.029$ m, and $\varepsilon_\psi = \pi/180$ radian. We performed the experiment under two conditions. Under condition 1, we set $\boldsymbol{p}_{\mathrm{front}} = \left[0.595,\, 0.146,\, 0.0970\right]^{\mathrm{T}}$ and $\boldsymbol{\theta}_{\mathrm{front}} = \left[-0.107,\, 0.00,\, 0.00\right]^{\mathrm{T}}$. Under condition 2, we set $\boldsymbol{p}_{\mathrm{front}} = \left[0.593,\, 0.140,\, 0.0673\right]^{\mathrm{T}}$ and $\boldsymbol{\theta}_{\mathrm{front}} = \left[0.00,\, -0.0609,\, 0.00\right]^{\mathrm{T}}$. Table 6 gives control parameters for each condition. We changed d_d, d_r, k_v, A depending on environment. d_d, d_r, k_v are changed depending on the gap between the front-plane and rear-plane, and A is changed depending on the inclination between the planes. In the proposed method, the robot lift the wheels of the connection-part by using the redundancy.

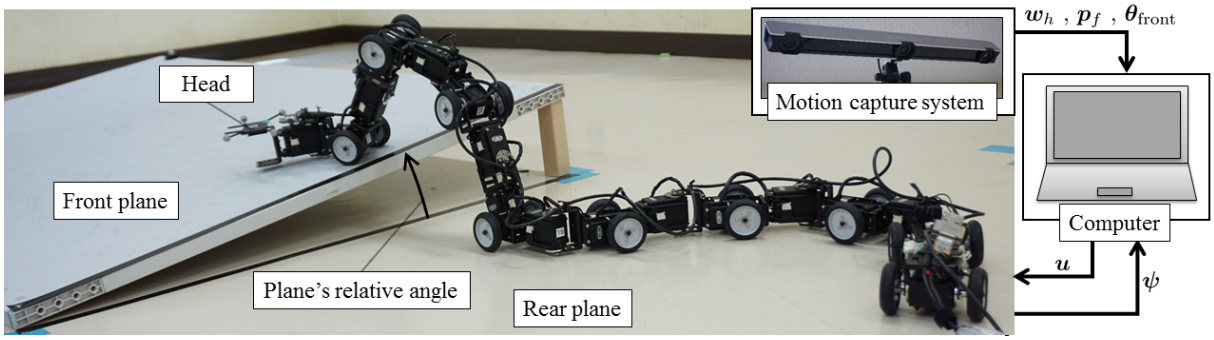

Figure 9. Experimental system

The height of the wheels which are lifted from the rear-plane depends on parameters of the evaluation function. If the height of wheels which are lifted from rear-plane is small, the robot comes into collision with the front-plane. d_d is the height which maximizes V_2, the element of evaluation function. When d_d is set large value, the wheels are lifted high. The gap between front-plane and rear-plane in condition 1 is larger than the gap in condition 2. Therefore, in condition 1, we set d_d larger than condition 2. d_r is a variable that determines the height which makes V_2 to zero. We changed d_r according to d_d. Because the wheels are lifted high in condition 1 compared to condition 2, motion of the joint of the connection-part becomes large compared to condition 2. Therefore, in condition 1, we set higher k_v than condition 2 for increasing the input of the connection part caused by redundancy. Also, the posture of the whole robot is important for the proplsion of the robot on the slope without slip. The large friction is generated in the lateral direction of the robot's trunk, and the small friction is generated in the longitudinal direction of the robot's trunk. For this reason, when the whole robot takes the small undulated posture as Figure 10(a), the component force of frictional force in the direction of travel of the robot becomes small. In contrast, when the whole robot takes the large undulated posture as Figure 10(b), the component force of frictional force in the direction of travel of the robot becomes large. The trunk of the robot follows a path closer to the path which the head of the robot followed. Thus, when the target trajectory of the head of the robot is set large undulated trajectory, the whole robot takes the large undulated posture. We set target trajectory of the head of the robot as sin curve and the amplitude of the curve is determined by A. Therefore, when A is set large, the component force of frictional force in the direction of travel of the robot becomes large. The inclined directions is orthogonal to the direction of travel of the robot in condition 1, and parallel to the direction of travel of the robot in condition 2. From this fact, in condition 2, we set the larger A than in condition 1. As a result, the component force of frictional force in the direction of travel of the robot becomes large, and the risk of sliding down are reduced. Designing a control method that is less dependent on the environment is one of future works.

Figures 11 and 12 show the experimental state and response of the controlled variable under conditions 1 and 2, respectively. The dotted line and solid line respectively indicate the target and measured values. The delimiting by dot-dash lines in Fig. 11(d) shows the times at which the controlled variable was switched by the transition of the rear end of the connection part. As shown in Figs. 11(a) and 12(a), the robot's head came into contact with the front plane through head adaptive motion. Furthermore, the connection part propagated backward. As shown in Figs. 11(c) and 12(c), the controlled variable for trajectory tracking $\boldsymbol{w}_h$ followed the target $\boldsymbol{w}_{h_d}$.

Table 1. Parameters of the controller

	d_d[m]	d_r[m]	$\boldsymbol{k}_c$	$\boldsymbol{k}_p$	k_v	g_1	g_2	v_p[m/s]	A[m]	T[sec.]
condition 1	0.272	0.272	$[1,1,1]$	$[1,1,1]$	3	0.7	0.3	0.01	0.25	90
condition 2	0.181	0.181	$[1,1,1]$	$[1,1,1]$	2	0.7	0.3	0.01	0.3	90

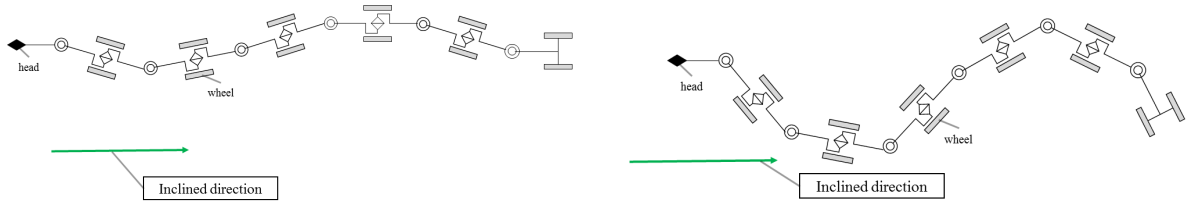

(a) Small friction posture

(b) Large friction posture

Figure 10. Posture of the whole robot

The robot's head thus followed the target trajectory on the front plane. Additionally, as shown in Figs. 11(b) and 12(b), although there was a difference between the target and actual values immediately after the beginning of motion, the controlled variable for head adaptive motion $\boldsymbol{r}_h$ generally followed the target $\boldsymbol{r}_{hd}$. The robot's head thus came into contact with the front plane via an appropriate posture. Immediately after the beginning of motion, the required torque of the connection-part joint discontinuously increased owing to the increasing number of wheels to be lifted. We consider that the cause of the error was the increase in torque. As shown in Figs. 11(d) and 12(d), the controlled variable for the connection part $\boldsymbol{r}$ converged to the target $\boldsymbol{r}_d$. The wheels were thus in contact with each plane with an appropriate posture under the action of the proposed controller of the connection part.

As achieved above, using the proposed control method, it is possible for the head of a snake robot to follow a target trajectory on two non-parallel planes. However, the proposed controller considers not dynamics but kinematics. It therefore seems that the robot cannot move forward in an environment that has a low friction coefficient or is greatly inclined from the horizontal plane because the velocity constraint of the wheel cannot be satisfied. Similarly, there is a possibility of falling because of the moment generated by the acceleration. Additionally, the proposed control method cannot be applied in an unknown environment because we assume that the parameters of the environment are given. Solving these problems remains as future work.

7. Conclusion

We proposed a motion control method for a snake robot moving between two non-parallel planes. We clarified the appropriate contact conditions for the environment and simplified the control model according to the conditions. In addition, we proposed a control method for trajectory tracking of the robot's head using a proposed model, and demonstrated its effectiveness by experiment. Future work is to realize propulsion on a slippery plane and to avoid falling considering the statics and dynamics.

Acknowledgment

This work was partially supported by the ImPACT Program of Council for Science, Technology and Innovation (Cabinet Office, Government of Japan). We thank Glenn Pennycook, MSc, from Edanz Group (www.edanzediting.com/ac) for editing a draft of this manuscript.

References

[1] Hirose S. Biologically Inspired Robots: Snake-like Locomotor and Manipulator. [place unknown]: Oxford University Press; 1993.

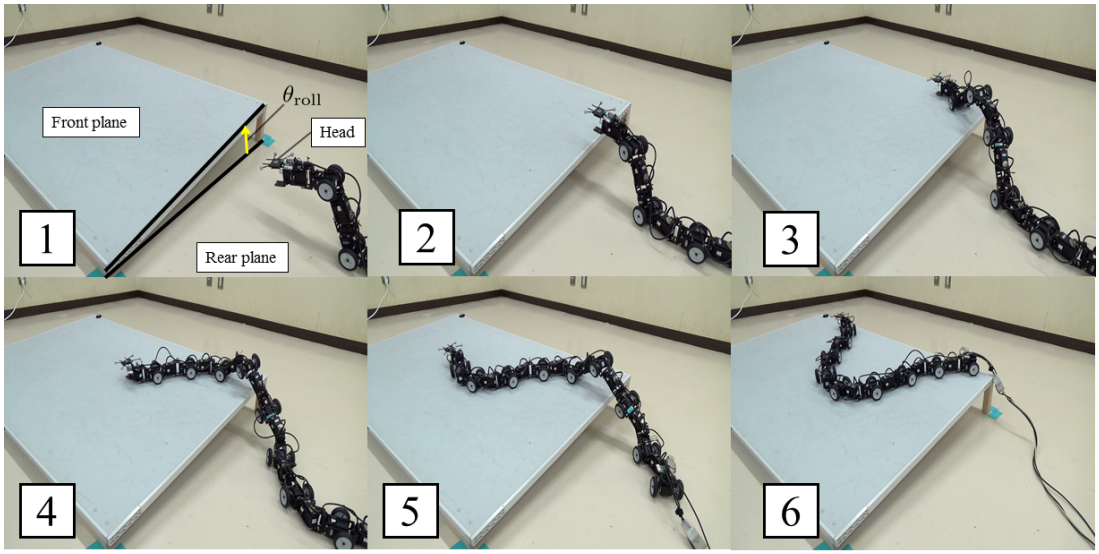

(a)

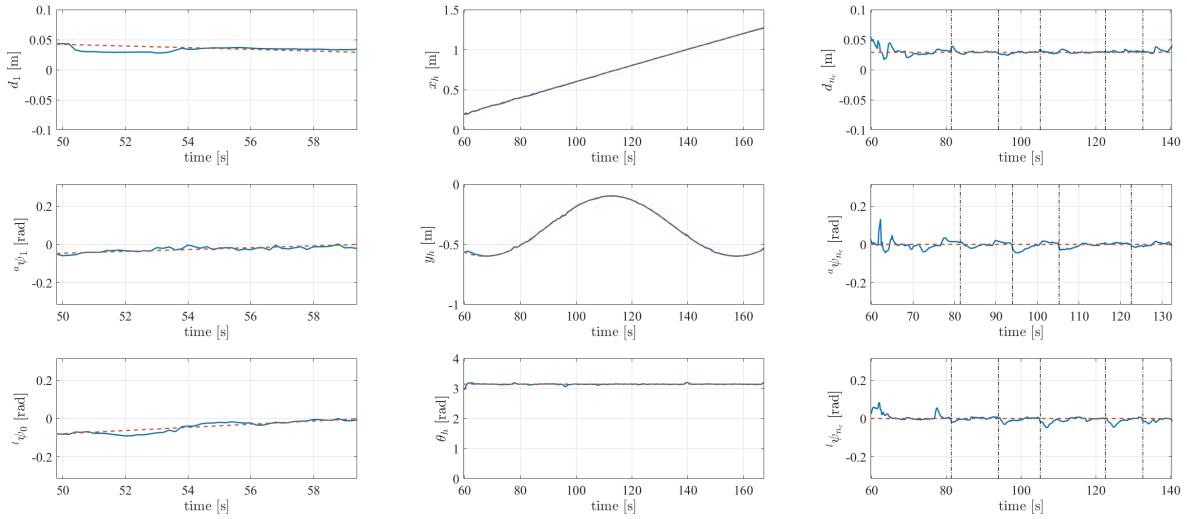

(b) (c) (d)

Figure 11. Experimental results for condition 1: (a) motion of the robot, (b) controlled variable of the head adaptive motion, (c) controlled variable of the motion for straddling two planes, and (d) controlled variable of the connection part

[2] Mori M, Hirose S. Three-dimensional serpentine motion and lateral rolling by active cord mechanism ACM-R3. In: Proceedings of the IEEE/RSJ International Conference on Intelligent Robots and Systems. Lausanne(CH); 2002. p.829-834.

[3] Ye C, Ma S, Li B, et al. Modular Universal Unit for a Snake-Like Robot and Reconfigurable Robots. Advanced Robotics. 2009;23(7-8):865-887.

[4] Liljebäck P, Haugstuen IU, Pettersen KY. Path Following Control of Planar Snake Robots Using a Cascaded Approach. IEEE Transaction on Control System Technology. 2012;20(1):111-126.

[5] Matsuno F, Mogi K. Redundancy controllable system and control of snake robot with redundancy based on kinematic model. In: Proceedings of the 39th IEEE Conference on Decision and Control. Sydney(AU); 2000. p.4791-4796.

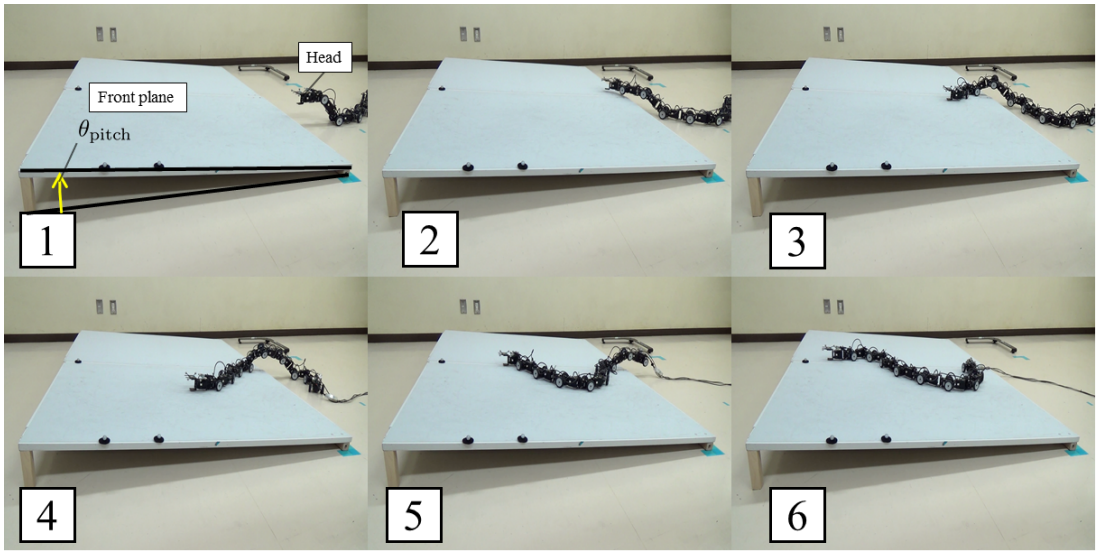

(a)

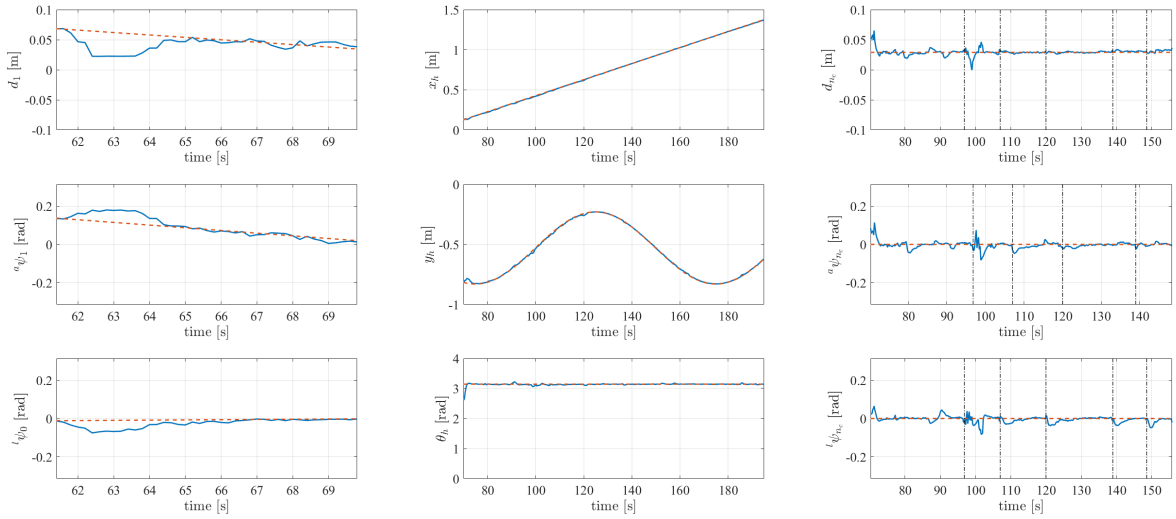

(b) (c) (d)

Figure 12. Experimental results for condition 2: (a) motion of the robot, (b) controlled variable of the head adaptive motion, (c) controlled variable of the motion for straddling two planes, and (d) controlled variable of the connection part

[6] Tanaka M, Matsuno F. Modeling and control of head raising snake robots by using kinematic redundancy. Journal of Intelligent and Robotic Systems. 2014;75(1):53-69.
[7] Huang K, Shao K, Zhen S, Sun H. A novel approavch for modeling and tracking control of a passive-wheel snake robot. Advances in Mechanical Engineering. 2017;9(3):1-15.
[8] Yamada H, Hirose S. [Study of active cord mechanism-approximations to continuous curves of a multi-joint body]. Journal of Robotics Society of Japan. 2008;26(1):110-120. Japanese.
[9] Tanaka M, Tanaka K. Control of a snake robot for ascending and descending steps. IEEE Transaction on Robotics. 2015;31(2):511-520.
[10] Kon K, Tanaka M, Tanaka M. Mixed Integer Programming-Based Semiautonomous Step Climbing of a Snake Robot Considering Sensing Strategy. IEEE Transaction on Control Systems Technology,

2016;24(1):252-264.
[11] Yamada H, Takaoka S, Hirose S. A snake-like robot for real-world inspection applications (the design and control of a practical active cord mechanism). Advanced Robotics. 2013;27(1):47-60.
[12] Shapiro A, Greenfield A, Choset H. Frictional Compliance Model Development and Experiments for Snake Robot Climbing. In: Proceedings of the IEEE Internetional Conference on Robotics and Automation. Roma(IT);2007. p.574-579.
[13] Barazandeh F, Bahr B, Moradi A. How Self-locking Reduces Actuators Torque In Climbing Snake Robots. In: Proceedings of IEEE International Conference on Advanced intelligent mechatronics. Zurixh(CH);2007. p.1-6.
[14] Date H, Takita Y. Control of 3D snake-like locomotive mechanism based on continuum modeling. In: Proceedings of ASME 2005 International Design Engineering Technical Conference. Long Beach(US);2005. p.1351-1359.
[15] Lipkin K, Brown I, Peck A, et al. Differentiable and piecewise differentiable gaits for snake robots. In: Proceedings of the IEEE/RSJ International Conference on Intelligent Robots and Systems. San Diego(US);2007. p.1864-1869.
[16] Kamegawa T, Harada T, Gofuku A. Realization of cylinder climbing locomotion with helical form by a snake robot with passive wheels. In: Proceedings of the IEEE International Conference on Robotics and Automation. Kobe(JP);2009. p.3067-3072.
[17] Hatton RL, Choset H. Generating gaits for snake robots: annealed chain fitting and keyframe wave extraction. Autonomous Robots. 2010;28(3):271-281.
[18] Rollinson D, Choset H. Gait-Based Compliant Control for Snake Robots. In: Proceedings of the IEEE International Conference on Robotics and Automation. Karlsruhe(DE);2013. p.5123-5128.
[19] Kamegawa T, Baba T, Gofuku A. V-shift control for snake robot moving the inside of a pipe with helical rolling motion. In: Proceedings of the IEEE International Symposium on Safety, Security and Rescue Robotics. Kyoto(JP);2011. p.1-6.
[20] Tsukano H, Tanaka M, Matsuno F. Control of a snake robot on a cylindrical surface based on a kinematic model. IFAC Proceedings Volumes. 2009;42(16):699-704.
[21] Tanaka M, Kon K, Tanaka K. Range-sensor-based Semiautonomous Whole-body Collision Avoidance of a Snake Robot. IEEE Transaction on Control Systems Technology. 2015;23(5):1927-1934.
[22] Ponte H, Queenan M, Gong C, et al. Visual Sensing for Developing Autonomous Behavior in Snake Robots. In: Proceedings of the IEEE International Conference on Robotics and Automation, Hong Kong(CN);2014. p.2779-2784.
[23] Liljebäck P, Stavdahl Ø, Pettersen KY, et al. Mamba - A Waterproof Snake Robot with Tactile Sensing. In: IEEE/RSJ International Conference on Intelligent Robots and Systems. Chicago(US);2015. p.294-301.
[24] Kouno K, Yamada H, Hirose S. Development of Active-Joint Active-Wheel High Traversability Snake-Like Robot ACM-R4.2. Journal of Robotics and Mechatronics. 2013;25(3):559-566.
[25] Pfotzer L, Staehler M, Hermann A, et al. KAIRO 3: Moving Over Stairs & Unknown Obstacles with Reconfigurable Snake-Like Robots. In: Proceedings of the European Conference on Mobile Robots. Lincoln(UK);2015. p.1-6.
[26] Ma S, Tadokoro N, Inoue K. Influence of the gradient of a slope on optimal locomotion curves of a snake-like robot. Advanced Robotics. 2006;20(4):413-428.
[27] Crespi A, Ijspeert AJ. Online optimization of swimming and crawling in an amphibious snake robot. IEEE Transaction on Robotics. 2008;24(1):75-87.
[28] Hatton RL, Choset H. Sidewinding on Slopes. In: Proceedings of the IEEE International Conference on Robotics and Automation. Anchorage(US);2010. p.691-696.
[29] Gong C, Tesch M, Rollinson D, et al. Snakes on an Inclined Plane: Learning an adaptive sidewinding motion for changing slopes. In: Proceedings of the IEEE International Conference on Intelligent Robots and Systems. Chicago(US);2013. p.1114-1119.
[30] Zheng YF, Shen J. Gait synthesis for the SD-2 biped robot to climb sloping surface. IEEE Transaction on Robotics and Automation. 1990;6(1):86-96.
[31] Grand C, Benamar F, Plumet F, et al. Stability and traction optimization of a reconfigurable wheel-legged robot. The International journal of Robotics Research. 2004;23(10-11):1041-1058.
[32] Nakamura Y, Hanafusa H, Yoshikawa T. Task-priority based redundancy control of robot manipulators. The International Journal of Robotics Research. 1987;6(2):3-15.